

---

# Exploiting GAN Internal Capacity for High-Quality Reconstruction of Natural Images

---

**Marcos Pividori\***  
Universidad Nacional de Rosario  
marcospividori@gmail.com

**Guillermo L. Grinblat** **Lucas C. Uzal**  
CIFASIS, UNR-CONICET  
{grinblat, uzal}@cifasis-conicet.gov.ar

## Abstract

Generative Adversarial Networks (GAN) have demonstrated impressive results in modeling the distribution of natural images, learning latent representations that capture semantic variations in an unsupervised basis. Beyond the generation of novel samples, it is of special interest to exploit the ability of the GAN generator to model the natural image manifold and hence generate credible changes when manipulating images. However, this line of work is conditioned by the quality of the reconstruction. Until now, only inversion to the latent space has been considered, we propose to exploit the representation in intermediate layers of the generator, and we show that this leads to increased capacity. In particular, we observe that the representation after the first dense layer, present in all state-of-the-art GAN models, is expressive enough to represent natural images with high visual fidelity. It is possible to interpolate around these images obtaining a sequence of new plausible synthetic images that cannot be generated from the latent space. Finally, as an example of potential applications that arise from this inversion mechanism, we show preliminary results in exploiting the learned representation in the attention map of the generator to obtain an unsupervised segmentation of natural images.

## 1 Introduction

The development of Generative Adversarial Networks (GAN) [1] represented a milestone in the problem of data generation, that is learning generative models that map samples from a simple latent distribution into samples of a complex data distributions such as natural images. In recent years several works have shown empirical results of applying these methods to different tasks. Recently, Brock et al. [2] demonstrated that it is possible to train GAN models on a larger scale and generate high-resolution diverse samples from complex datasets such as ImageNet [3], with remarkable results.

The representation learned by the generator captures meaningful semantic variations along the data distribution [4]. Therefore, it is desirable to exploit this learned representation. In particular, there has been a recent interest in making use of the capability of the generator to approximate the manifold of natural images (semantic image editing) [5] [6], projecting real images into the latent space and manipulating them to produce smooth visual changes over high level features, preserving the realism of the result. This requires the initial step of obtaining a reconstruction close to the original image. However, the GAN framework lacks an automatic inference mechanism, which represents a bottleneck in these cases. Inverting the generator is not a trivial operation, specially when it is a complex model. Furthermore, it is frequently observed that real images cannot be represented in the latent space, obtaining approximations with a high reconstruction error, which limits the positive impact of being able to make semantic edits.

---

\*This preprint is the result of the work done for the undergraduate dissertation of M. Pividori supervised by L.C. Uzal and G.L. Grinblat, and presented in July 2019.

When there is no latent value that permits to reconstruct the image, it is generally considered to be evidence that the generator cannot model certain image attributes [7], commonly referred to as mode dropping. In this work, we demonstrate that in many of these cases, modes can be modeled in the internal layers of the generator, but this capacity is not exploited from the latent space. In particular, we show the importance of the learned representation after the first dense layer of the generator, since it is very expressive and allows to represent arbitrary natural images with high visual fidelity. We also propose an inversion algorithm which permits to find meaningful representations, in the sense that we can perform interpolation experiments around those images obtaining a full sequence of new valid synthetic images that cannot be generated from the latent space. By allowing to reconstruct much better the real images, our work has direct impact on all previous work on high-level image editing and processing using the GAN generator [5] [6] [8].

In addition, we demonstrate that a generator of the complexity of BigGAN [2] can be inverted with a non-parametric approach while previous works [5] [9] [10] mostly consider simple DCGAN models and datasets of low variability. Finally, as a new practical application, we show that it is possible to exploit the learned representation in the attention map of the generator to obtain an unsupervised segmentation of real images.

## 2 Related work

Since the development of GAN there has been a general interest in inverting the generator and exploiting the representation that was learned in an unsupervised manner. For example, for retrieval and classification [4], to manipulate images [5] [6], and to provide relevant insights on which features the generator has learned to model [9].

Inverting the generator implies finding a vector  $z \in \mathcal{Z}$  that when provided as input results in a image  $G(z)$  that is very close to the target image. Mapping an image from pixel space to latent space is not a trivial operation, as it requires inverting the generator, which usually consists of a complex model of several non-linear layers. In addition, the same image could be generated from different  $z$  values or none at all. In their original formulation, GANs do not provide a direct inference mechanism. In this direction, previous works can be grouped into two main approaches:

**Parametric models** A line of work proposes to learn a parametric model (encoder) that maps each image to a representation in the latent space  $\mathcal{Z}$ . Donahue et al. [11] and Dumoulin et al. [12] proposed to train the encoder jointly with the generator and discriminator, in an adversarial setup. Other works considered training the encoder on a pre-trained generator, through a regression in the  $\mathcal{Z}$  space [11], or in the space of images [13].

In general, these approaches have the disadvantage of requiring the training of a third model (encoder), increasing the number of parameters to be learned and the risk of overfitting or underfitting (depending on the training method). Although good results have been shown when using the encoder as a feature extractor for classification tasks, in general reconstructions are not good, failing to preserve the structure and style of images. Finally, introducing a complex model to invert the generator makes it questionable as a diagnostic tool to evaluate the representation of the generator [9].

**Optimization on the generator** Creswell and Bharath [9] proposed to find the  $z$  vector that generates a certain image  $x$ , solving an optimization problem over the generator. Essentially, they follow the gradient of the generator  $G$  with respect to its input. Zhu et al. [5] includes a similar approach as part of larger framework to manipulate images. Lipton and Tripathi [10] proposed an extension to improve the recovery in cases of uniform prior distribution on the latent space. A similar algorithm was previously proposed by Mahendran and Vedaldi [14] to study the representation of deep networks.

Our work focuses on the study of the intermediate representations of the generator, the invertibility of the different layers and the degree of reconstruction of real images. We opt to use the optimization approach on the generator, since it does not require the introduction and training of a new set of parameters for modelling the inverse function, which could weaken the conclusions that can be drawn from the results.

Unlike previous work, we conduct our experiments on ImageNet [3], which provides wider variability, including different classes of objects in different situations, and therefore the model has to deal with

greater complexity. The methods mentioned above do not perform well or directly do not show results on this more complex dataset. Moreover, previous work on non-parametric approaches only consider simple DCGAN models, while we demonstrate that we can invert much deeper generators (BigGAN), which makes the inversion much more challenging. In addition, we propose to extend this inversion mechanism to the hidden layers of the generator, showing the advantages of using the learned representation in the first fully connected layer, where it is possible to reconstruct natural images with high visual fidelity while still capturing high-level features.

### 3 Inverting the generator to intermediate layers

Let  $G : \mathcal{Z} \rightarrow \mathcal{X}$  be a generator of deep architecture, composed of  $n$  layers, that transforms a latent vector  $z \in \mathbb{R}^{d_z}$  sampled from a distribution  $z \sim P_z$  to an image  $\hat{x} = G(z)$ , with an implicit distribution  $P_{model}$  that approximates  $P_{data}$ , the distribution of real data on the image space  $\mathcal{X} = \mathbb{R}^{W \times H \times C}$ .

We can split the generator in a given hidden layer  $l$  (with dimensionality  $d_l$ ), and analyze the learned representation at that point, redefining the generator as the composition of two generators:

$$G(z) = G_2^l(G_1^l(z))$$

where  $G_1^l : \mathcal{Z} \rightarrow \mathbb{R}^{d_l}$  represents the transformation from latent space to layer  $l$ , and  $G_2^l : \mathbb{R}^{d_l} \rightarrow \mathcal{X}$  from layer  $l$  to the space of images  $\mathcal{X}$ .

Let  $P_h^l$  be the generated distribution in the hidden layer  $l$  ( $\mathbb{R}^{d_l}$ ) according to the random variable  $H_{gen}^l = G_1^l(z)$  with  $z \sim P_z$ . Then, we can consider  $G_2^l(h)$  as a generator from the learned latent distribution  $h \sim P_h^l$ , which has the same performance as the original generator  $G(z)$  with  $z \sim P_z$ .

#### 3.1 Invertibility of the generator

We say that  $G$  is invertible in a set of images  $S$  if it is right invertible, that is, if there is a function  $G^{-1} : S \rightarrow \mathcal{Z}$  such that  $G(G^{-1}(x)) = x \ \forall x \in S$ . An optimal generator, that is, that can generate the target distribution in the output space ( $P_{model} = P_{data}$ ), is invertible on real images.

**Theorem 1.** *An optimal generator  $G^*$  is right invertible  $P_{data}$ -almost everywhere in  $\mathcal{X}$ .*

*Proof.* Let  $\mathcal{X}' = \mathcal{X} - G^*(\mathcal{Z})$  be the set of images that can not be generated. Then  $\mathcal{X}'$  has measure zero under  $P_{data}$ , therefore  $G^*$  is right invertible  $P_{data}$ -almost everywhere in  $\mathcal{X}$ .

$$P_{data}(\mathcal{X}') = P_{model}(\mathcal{X}') = 0 \quad \square$$

For a non-optimal generator, we expect real images to be approximately invertible, where the reconstruction quality depends on the layer considered for the representation. At the output layer, it is possible to represent all images with zero reconstruction error. As we move in the network backwards (considering the input space of  $G_2^l$  for some layer  $l$ ), the reconstruction error for certain images is expected to increase.

Since in the generator the information flows forward, every image represented in a given layer has no better representation in previous layers, and at least as good in the following layers. If we consider two layers  $l < m$ , the image set of  $G_2^l$  is a subset of the image set of  $G_2^m$  ( $G_2^l(\mathbb{R}^{d_l}) \subseteq G_2^m(\mathbb{R}^{d_m})$ ). Then, the closer to the latent space, the more restricted the image set  $G_2^l(\mathbb{R}^{d_l})$  at pixel level, which means that more images are filtered out. It would be expected that in a properly trained generator, the increase in reconstruction error is manifested mainly in irrelevant areas of the distribution at pixel level (e.g. white noise images) and to a much less extent in natural images.

#### 3.2 First dense layer

In particular, in this work we are interested in analyzing the learned representation in the first dense layer (included in all the state-of-the-art GAN architectures). Suppose the first layer of the generator has  $d_1$  fully connected units, then we split the generator at this point:

$$G_1^1(z) = W_1 z + b_1$$

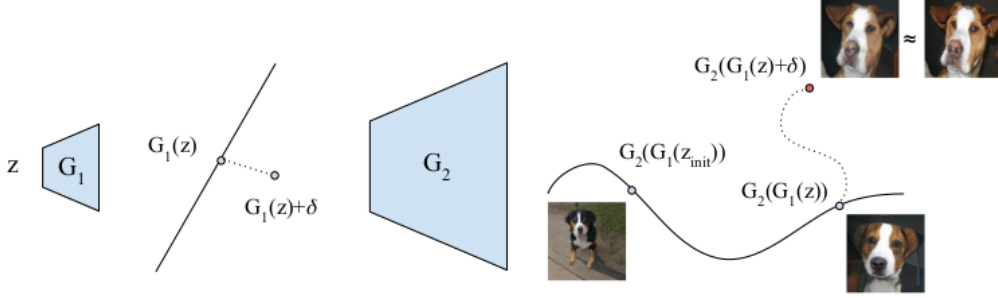


Figure 1: Interpretation of the two-step optimization at different levels of representation. In the space of the first layer, the linear subspace  $G_1(\mathcal{Z})$  is considered first, then the displacement  $\delta$  permits to explore the whole space. In pixel-level, first we find the best approximation in the generated manifold  $G(\mathcal{Z})$  and then  $\delta$  involves considering the directions captured by the manifold  $G_2(\mathbb{R}^d)$ .

where  $W_1 \in \mathbb{R}^{d_1 \times d_z}$ .  $G_1^1(\mathcal{Z})$  represents a linear subspace of dimensionality at most  $d_z$  (column space of  $W_1$ ) in  $\mathbb{R}^{d_1}$ . In general  $d_1$  is one or two orders of magnitude greater than  $d_z$ .

From now on, we omit the index  $l$  as we will always consider the first fully connected layer (e.g.  $G_1$  denotes the first linear mapping  $G_1^1$  and  $G_2$  the rest of the network  $G_2^1$ ), although most of the concepts can be extended to other intermediate layers. The output space  $\mathbb{R}^{d_1}$  is referred to as *the space of the dense layer*.

### 3.3 Proposed algorithm

Given a generator  $G$  whose computational graph is differentiable, we want to infer a representation  $h$  in the space of the first layer that makes it possible to reconstruct a target image  $x \in \mathcal{X}$ , guided by the gradient  $\nabla_h \mathcal{L}(G_2(h), x)$ .  $\mathcal{L}$ , the loss to minimize, represents the reconstruction error between the generated and target image. In other words, we approximate the following optimization by gradient descent:

$$h^* = \arg \min_{h \in \mathbb{R}^d} \mathcal{L}(x, G_2(h)).$$

The space of the first dense layer is of a much greater dimensionality than that of the generated linear subspace  $G_1(\mathcal{Z})$ , therefore the capacity of representation is considerably more extensive. When optimizing in the space of the dense layer without regularization, the algorithm obtains representations that, although map to the target image, are not related to the distribution of points generated in this space of the network during training. As a result, the obtained representation is poor and does not seem to capture the factors of variation in the data. For example when shifting the vector in any direction, the image degrades.

Instead, it is desirable to choose, among all possible representations of an image, the one closest to the generated distribution ( $P_h$ ), where the generator was adjusted to output plausible samples. Then, we propose to optimize on  $G_2(G_1(z) + \delta)$  where  $\delta$  represents a displacement in the first layer with respect to the point  $G_1(z)$ . The optimization is split into two steps, first the reconstruction error on the latent vector is optimized:

$$z^* = \arg \min_{z \in \mathcal{Z}} \mathcal{L}(x, G_2(G_1(z))) - \lambda_1 \log P_z(z)$$

Then, it is optimized over a displacement in the full space of the dense layer:

$$\delta^* = \arg \min_{\delta \in \mathbb{R}^d} \mathcal{L}(x, G_2(G_1(z^*) + \delta)) + \lambda_2 \|\delta\|_1$$

Obtaining the final representation  $h^* = G_1(z^*) + \delta^*$ .

**Regularization in  $z$ .** The term  $\log P_z(z)$  represents the log likelihood of  $z$ , and regularizes the search in the latent space to ensure that the optimization stays within probable regions of  $\mathcal{Z}$ , as proposed in [9]. For example, if the network is trained with  $z \sim \mathcal{N}(0, I)$ , the log likelihood reduces to a regularization in  $\|z\|_2^2$ .

**Regularization in  $\delta$ .** In a space of such high dimensionality as the first layer, we choose the  $l_1$  norm to regularize  $\delta$  because it encourages sparse solutions, including the least amount of non-zero components necessary to properly approximate the target image.

We can analyze this two-step optimization in the space of the dense layer. First, when optimizing up to the latent space, only points of the linear subspace  $G_1(\mathcal{Z})$  are considered. Moreover, if the first linear mapping  $G_1$  is injective (a reasonable assumption), optimizing  $G_2(G_1(z))$  with a regularization term in the log likelihood of  $z$  is equivalent to optimizing  $G_2(h)$  over the entire space  $\mathbb{R}^d$  of the dense layer, with a regularization in the log likelihood of  $h$  with respect to the generated distribution  $P_h$ .

**Theorem 2.** *If the first linear mapping  $G_1$  is injective:*

$$\arg \min_{h \in \mathbb{R}^d} \mathcal{L}(x, G_2(h)) - \lambda_1 \log P_h(h) = G_1(\arg \min_{z \in \mathcal{Z}} \mathcal{L}(x, G_2(G_1(z))) - \lambda_1 \log P_z(z))$$

*Proof.*

$$\begin{aligned} & \arg \min_{h \in \mathbb{R}^d} \mathcal{L}(x, G_2(h)) - \lambda_1 \log P_h(h) \\ &= \arg \min_{h \in G_1(\mathcal{Z})} \mathcal{L}(x, G_2(h)) - \lambda_1 \log P_h(h) && (P_h(h) = 0 \quad \forall h \in \mathbb{R}^d - G_1(\mathcal{Z})) \\ &= \arg \min_{h \in G_1(\mathcal{Z})} \mathcal{L}(x, G_2(G_1(G_1^{-1}(h)))) - \lambda_1 \log (P_z(G_1^{-1}(h)) \frac{1}{|\det(\frac{\partial G_1(G_1^{-1}(h))}{\partial G_1^{-1}(h)})|}) && (G_1 \text{ injective}) \\ &= \arg \min_{h \in G_1(\mathcal{Z})} \mathcal{L}(x, G_2(G_1(G_1^{-1}(h)))) - \lambda_1 \log \frac{P_z(G_1^{-1}(h))}{|\det(W_1)|} \\ &= \arg \min_{h \in G_1(\mathcal{Z})} \mathcal{L}(x, G_2(G_1(G_1^{-1}(h)))) - \lambda_1 \log P_z(G_1^{-1}(h)) + \lambda_1 \log |\det(W_1)| \\ &= \arg \min_{h \in G_1(\mathcal{Z})} \mathcal{L}(x, G_2(G_1(G_1^{-1}(h)))) - \lambda_1 \log P_z(G_1^{-1}(h)) \\ &= G_1(\arg \min_{z \in \mathcal{Z}} \mathcal{L}(x, G_2(G_1(z))) - \lambda_1 \log P_z(z)) \quad \square \end{aligned}$$

Then, in the second step of the optimization, the displacement  $\delta$  exploits the internal capacity of the generator, considering all the space in the first layer ( $\mathbb{R}^d$ ), permitting to combine the features independently, out of the linear restriction established by the mapping  $G_1$ . Note that this involves generating images that cannot be generated from the latent space.

The coefficient  $\lambda_2$  represents a compromise between the quality of reconstruction and the quality of the obtained representation. Larger values of  $\lambda_2$  mean that the obtained representation remains close to the generated distribution, but the reconstruction may not be that close to the target image. On the other hand, as the value of  $\lambda_2$  decreases, the optimization displaces to a greater extent over the whole space of the first layer and therefore, even though the reconstruction ( $\hat{x}$ ) resembles the original image ( $x$ ), the obtained representation ( $h$ ) may not be as meaningful.

The two-step optimization can be interpreted in the output space of the generator (Figure 1). First we look for the best approximation of the target image considering  $d_z$  directions in the generated manifold  $G(\mathcal{Z})$ . Then, starting from this point, we extend the search to all the directions along the manifold  $G_2(\mathbb{R}^d)$ , looking for the simplest way to get to the target image, that is, the one that involves moving in the least amount of possible directions.

## 4 Experiments with the BigGAN generator

Prior work on inverting GAN generators with non-parametric approaches only consider simple DCGAN models and datasets of low variability [9] [10]. When attempting to invert more complex models such as BigGAN, the problem is more challenging, as the function to be optimized ( $\mathcal{L}(x, G(z))$ ) seems to be highly non-convex, conditioning the result of the optimization. In the following experiments <sup>2</sup>, we consider the pre-trained class-conditional BigGAN model trained on ImageNet for an image resolution of 128x128, publicly available<sup>3</sup>.

<sup>2</sup>Source code is available at: <https://github.com/CIFASIS/exploiting-gan-internal-capacity>

<sup>3</sup><https://tfhub.dev/deepmind/biggan-128/2>

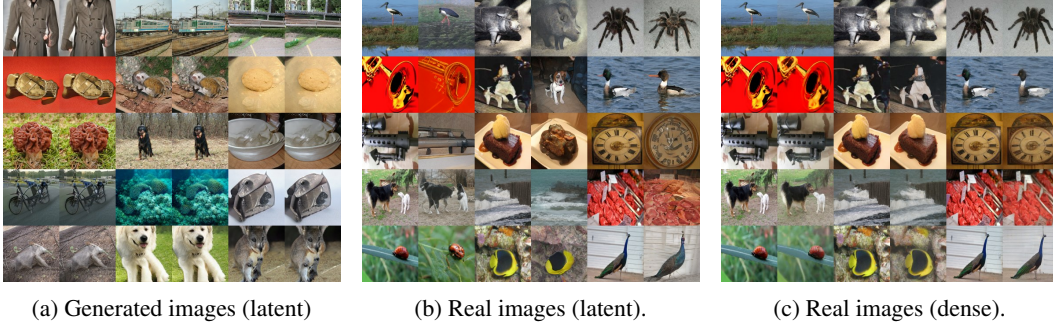


Figure 2: Results of inverting of BigGAN for a random sample of images. Generated images can be reconstructed with high fidelity to the latent space (a). For real images, reconstructions to the latent space (b) are semantically related to the target image. The quality of the reconstructions is improved when considering the representation in the first dense layer (c).

#### 4.1 Reconstruction error

We found in preliminary experiments that by simply optimizing over the Mean Square Error (MSE) at pixel level it is not possible to recover the representation of generated images ( $z$ ), since the optimization frequently gets stuck in non-optimal critical points. Metrics that compare images pixel-by-pixel, such as MSE, do not capture very well the similarity of images according to our perception of natural images [15]. As proposed in [16] [17], some invariance to irrelevant transformations and at the same time sensitivity to important image properties, such as edges and textures, can be achieved through the use of metrics in a higher level feature space, extracted by convolutional networks.

Let  $C_l$  represent the activation at the layer  $l$  of the InceptionV3 [18] network trained to classify ImageNet, then we propose to compare two images considering the euclidean distance in the feature space:  $\|C_l(x) - C_l(\hat{x})\|_2$ . Given that different layers capture different levels of complexity [19], after considering the layers of the InceptionV3 network, best results were achieved when comparing images at the representation of layer 7 (*Mixed\_7a*), with a compromise between generalization and preservation of the visual structure of the images. Then, we define the reconstruction error as a linear combination of the MSE and the distance in the feature space extracted by the InceptionV3 network:

$$\mathcal{L}_{mse-feat}(x, \hat{x}) = \|x - \hat{x}\|_2^2 + \lambda_{feat} \|C(x) - C(\hat{x})\|_2^2$$

Following the hypothesis [20] that deeper representations unfold the manifolds on which real data is concentrated, one could hypothesize that the representation learned by a deep network trained on the set of real images (for example InceptionV3) succeeds in disentangling the manifold of natural images and, therefore, also the generated manifold  $G(\mathcal{Z})$  that attempts to approximate it. This is consistent with the empirical results: the euclidean distance at the level of features extracted by a deep network provides better gradients that allow to traverse the generated manifold until recovering the latent vector of generated images.

#### 4.2 Inverting generated images

Before drawing conclusions about the representational power of different layers of the network, it is important to ensure that the inversion mechanism works correctly, verifying that it is possible to recover generated images for which exists an input value that perfectly maps to the target image.

Considering the generated distribution  $P_{model}$  as a baseline, 1000 images were generated ( $x \sim P_{model}$ ) and inverted to the latent space minimizing the reconstruction error  $\mathcal{L}_{mse-feat}$  with a regularization on the log likelihood. As can be observed in Figure 2a, it is possible to reconstruct the images to an insignificant reconstruction error which confirms that the inversion algorithm is working properly.

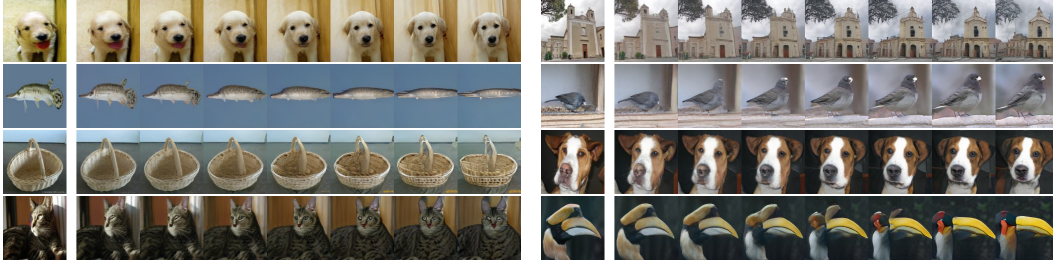


Figure 3: Left: Real image. Right: Linear interpolation between its closest reconstruction in the first step of the optimization ( $G_2(G_1(z^*))$ , right) and the closest reconstruction in the second step ( $G_2(G_1(z^*) + \delta^*)$ , left). Note that except from the right-most column, the rest of intermediate images can not be generated from the latent space.



Figure 4: Linear interpolation between the reconstruction of two real images for the same class. First row: reconstruction in the latent space. Second row: reconstruction in the dense layer without regularization. Third row: reconstruction in the dense layer with the proposed two-step optimization.

### 4.3 Inverting natural images

Next, the distribution of natural images  $P_{data}$  is considered, sampling 1000 random images of ImageNet ( $x \sim P_{data}$ ), and inverting them following the proposed two-step optimization on the reconstruction error  $\mathcal{L}_{mse-feat}$ .

In the first step of the optimization (up to the latent space) we obtain reconstructions that are semantically related to the target image although they differ substantially (Figure 2b). Since the inversion mechanism works correctly for generated images, we can conclude that a high reconstruction error is obtained for real images because they cannot be represented in the latent space. When the second step of the optimization is performed, including a displacement  $\delta$  over the entire space of the dense layer, the reconstruction error is considerably reduced, obtaining high-quality reconstructions (Figure 2c).

As shown in Figure 5, there is a significant gap between the reconstruction error over real images at the two levels of the network, demonstrating the difference in the power of representation of natural images. In the first dense layer, natural images can be represented with a low reconstruction error, similar to generated images.

At the same time, representations obtained in the first layer are meaningful, as can be seen when interpolating linearly with generated images (Figure 3) and with the representation of other natural images of the same class (Figure 4), producing a smooth transition. It should be noted that all intermediate images resulting from these interpolations cannot be generated from the latent space, as they are outside the linear subspace  $G_1(\mathcal{Z})$ . This demonstrates that the generator has a greater exploitable capacity to generate images than what is captured by the latent space.

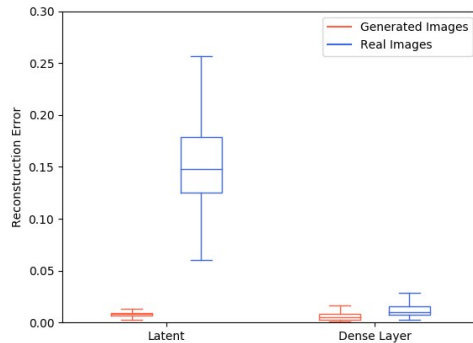


Figure 5: Reconstruction error ( $\mathcal{L}_{mse-feat}$ ) for a random sample of 1000 generated and 1000 real images, at different levels of representation.



Figure 6: Examples of unsupervised segmentation (64x64) for real images, after inverting the generator to the first layer (different numbers of clusters: 8, 20, 40). Only for visualization purposes, each cluster is associated to the average color of all its pixel members.

## 5 Unsupervised segmentation

Inverting the generator on natural images means learning to generate them, and the structure of the network can provide information on what the components of the images are and how they relate to each other. As an example of potential application, we show that the learned representation in the self-attention map of the generator [21] [22] can be exploited to obtain an unsupervised segmentation of real images. We consider the Embedded Gaussian variant of the non-local block [22], as employed in BigGAN. Given input feature vectors  $x_i$  ( $i$  index over  $N$  spacial positions) the attention matrix  $A \in \mathbb{R}^{N \times N}$  is defined as:

$$A_{ij} = \frac{e^{\psi(x_j)^T \phi(x_i)}}{\sum_j e^{\psi(x_j)^T \phi(x_i)}}$$

where  $\psi(x) = W_\psi x$  and  $\phi(x) = W_\phi x$  are two embedding spaces.  $A_{ij}$  indicates the attention on position  $j$  when computing the output of position  $i$ . Using this learned attention map, we propose to define a dissimilarity matrix  $D \in [0, 1]^{N \times N}$  between different points of the image:

$$D = \left(1 - \frac{A + A^T}{2}\right) \odot (1 - I).$$

In this way, the matrix is symmetric and the dissimilarity of a point with itself is minimum.

In particular, for BigGAN on 128x128 resolution, the non-local block is included at 64x64 resolution, and contains a max pooling intermediate layer (Subsampling Trick [22]). A 32x32 attention map is computed for each point of the 64x64 resolution, determining how much attention to pay to each section of the 32x32 resolution. Therefore, we upsample it spatially to a 64x64 map, and then compute the dissimilarity matrix.

Then, we apply Agglomerative Hierarchical Clustering to the dissimilarity matrix  $D$ , with average linkage as link criteria between different clusters. This can be interpreted as joining clusters on the basis of the average attention paid to each other. Resulting clusters represent an unsupervised segmentation of the image at the resolution of the attention map (64x64 in our example).

Therefore, given a high quality reconstruction of a real image, it is possible to segment the image using the structure of the network. As shown in the Figure 6, although not perfect, resulting clusters group significant sections of the image associated with the same concept.

## 6 Conclusion

The possibility of accessing to high-level representations of natural images and their respective reconstructions allows for countless image processing and editing applications based on manipulation of semantic features. The success of these applications is limited by the quality of the reconstruction and the quality of the reached representation.

In this work we have shown that it is possible to reach *good* representations of real natural images in the space after the first layer of a GAN generator. These are good representations in the sense that, on one hand, we can obtain high-quality reconstructions of the images and, on the other hand, we can



perform interpolation experiments in the representation space obtaining a full sequence of plausible images from any real image to a target image (real or generated).

All the experiments were performed using the state-of-the-art BigGAN generator and the ImageNet dataset, which is the most challenging scenario. Finally, as a further example of potential application, we also showed that the learned representation in the self-attention map of the generator can be exploited to obtain an unsupervised segmentation of real images.

### Acknowledgments

The authors acknowledge grant support from ANPCyT PICT-2016-4374 and ASaCTeI IO-2017-00218. The Titan Xp used for this research was donated by the NVIDIA Corporation.

### References

- [1] Ian Goodfellow, Jean Pouget-Abadie, Mehdi Mirza, Bing Xu, David Warde-Farley, Sherjil Ozair, Aaron Courville, and Yoshua Bengio. Generative adversarial nets. In *Advances in neural information processing systems*, pages 2672–2680, 2014.
- [2] Andrew Brock, Jeff Donahue, and Karen Simonyan. Large scale gan training for high fidelity natural image synthesis. *arXiv preprint arXiv:1809.11096*, 2018.
- [3] Olga Russakovsky, Jia Deng, Hao Su, Jonathan Krause, Sanjeev Satheesh, Sean Ma, Zhiheng Huang, Andrej Karpathy, Aditya Khosla, Michael Bernstein, et al. Imagenet large scale visual recognition challenge. *International journal of computer vision*, 115(3):211–252, 2015.
- [4] Alec Radford, Luke Metz, and Soumith Chintala. Unsupervised representation learning with deep convolutional generative adversarial networks. *arXiv preprint arXiv:1511.06434*, 2015.
- [5] Jun-Yan Zhu, Philipp Krähenbühl, Eli Shechtman, and Alexei A Efros. Generative visual manipulation on the natural image manifold. In *European Conference on Computer Vision*, pages 597–613. Springer, 2016.
- [6] Andrew Brock, Theodore Lim, James M Ritchie, and Nick Weston. Neural photo editing with introspective adversarial networks. *arXiv preprint arXiv:1609.07093*, 2016.
- [7] Luke Metz, Ben Poole, David Pfau, and Jascha Sohl-Dickstein. Unrolled generative adversarial networks. *arXiv preprint arXiv:1611.02163*, 2016.
- [8] Raymond A Yeh, Chen Chen, Teck Yian Lim, Alexander G Schwing, Mark Hasegawa-Johnson, and Minh N Do. Semantic image inpainting with deep generative models. In *Proceedings of the IEEE Conference on Computer Vision and Pattern Recognition*, pages 5485–5493, 2017.
- [9] Antonia Creswell and Anil Anthony Bharath. Inverting the generator of a generative adversarial network. *IEEE transactions on neural networks and learning systems*, 2018.
- [10] Zachary C Lipton and Subarna Tripathi. Precise recovery of latent vectors from generative adversarial networks. *arXiv preprint arXiv:1702.04782*, 2017.
- [11] Jeff Donahue, Philipp Krähenbühl, and Trevor Darrell. Adversarial feature learning. *arXiv preprint arXiv:1605.09782*, 2016.
- [12] Vincent Dumoulin, Ishmael Belghazi, Ben Poole, Olivier Mastropietro, Alex Lamb, Martin Arjovsky, and Aaron Courville. Adversarially learned inference. *arXiv preprint arXiv:1606.00704*, 2016.
- [13] Junyu Luo, Yong Xu, Chenwei Tang, and Jiancheng Lv. Learning inverse mapping by autoencoder based generative adversarial nets. In *International Conference on Neural Information Processing*, pages 207–216. Springer, 2017.
- [14] Aravindh Mahendran and Andrea Vedaldi. Understanding deep image representations by inverting them. In *Proceedings of the IEEE conference on computer vision and pattern recognition*, pages 5188–5196, 2015.

- [15] Zhou Wang and Alan C Bovik. Mean squared error: Love it or leave it? a new look at signal fidelity measures. *IEEE signal processing magazine*, 26(1):98–117, 2009.
- [16] Justin Johnson, Alexandre Alahi, and Li Fei-Fei. Perceptual losses for real-time style transfer and super-resolution. In *European conference on computer vision*, pages 694–711. Springer, 2016.
- [17] Alexey Dosovitskiy and Thomas Brox. Generating images with perceptual similarity metrics based on deep networks. In *Advances in neural information processing systems*, pages 658–666, 2016.
- [18] Christian Szegedy, Vincent Vanhoucke, Sergey Ioffe, Jon Shlens, and Zbigniew Wojna. Rethinking the inception architecture for computer vision. In *Proceedings of the IEEE conference on computer vision and pattern recognition*, pages 2818–2826, 2016.
- [19] Ian Goodfellow, Honglak Lee, Quoc V Le, Andrew Saxe, and Andrew Y Ng. Measuring invariances in deep networks. In *Advances in neural information processing systems*, pages 646–654, 2009.
- [20] Yoshua Bengio, Grégoire Mesnil, Yann Dauphin, and Salah Rifai. Better mixing via deep representations. In *International conference on machine learning*, pages 552–560, 2013.
- [21] Han Zhang, Ian Goodfellow, Dimitris Metaxas, and Augustus Odena. Self-attention generative adversarial networks. *arXiv preprint arXiv:1805.08318*, 2018.
- [22] Xiaolong Wang, Ross Girshick, Abhinav Gupta, and Kaiming He. Non-local neural networks. In *Proceedings of the IEEE Conference on Computer Vision and Pattern Recognition*, pages 7794–7803, 2018.

Supplementary Material of

# Exploiting GAN Internal Capacity for High-Quality Reconstruction of Natural Images

Source code for reproducing the experiments is available at:

<https://github.com/CIFASIS/exploiting-gan-internal-capacity>

## Linear interpolation in the space of the dense layer

We show more examples of linear interpolation in the space of the dense layer, as a demonstration of the quality of obtained representations with the proposed two-step optimization. Note that all intermediate images of these interpolations can not be generated from the latent space.

**Representation gap.** Figure 7 shows examples of linear interpolation between the best reconstruction in the latent space and the best reconstruction in the space of the dense layer:

$$G_2(G_1(z^*) + \alpha \delta^*) \quad \text{with } \alpha \in [0, 1].$$

**Intra class interpolation.** Figure 8 shows examples of linear interpolation between two reconstructions of different real images ( $x_1$  and  $x_2$ ) in the same class:

$$G_2(\alpha h_1 + (1 - \alpha) h_2) \quad \text{with } \alpha \in [0, 1]$$

where  $h_1 = G_1(z_1^*) + \delta_1^*$  and  $h_2 = G_1(z_2^*) + \delta_2^*$  are the obtained representations of  $x_1$  and  $x_2$  in the space of the dense layer.

**Random interpolation.** Figure 9 shows examples of linear interpolation between the inverted real image and random generated images in the same class:

$$G_2(\alpha h_1 + (1 - \alpha) h_2) \quad \text{with } \alpha \in [0, 1]$$

where  $h_1 = G_1(z^*) + \delta^*$  and  $h_2 = G_1(z)$ ,  $z \sim \mathcal{N}(0, 1)$ .

## Unsupervised segmentation

Figure 10 includes more examples of segmented real images, clustering the self-attention map in the non-local block of BigGAN [2]. First, images are inverted to the dense layer with the two-step optimization, obtaining a representation  $h^* = G_1(z^*) + \delta^*$ . Let  $G_{att} : \mathbb{R}^d \rightarrow \mathbb{R}^{N \times N}$  represent the mapping from the dense layer to the attention map. Then, we cluster the output of  $G_{att}(h^*)$  and generate a segmentation of the image.

## Additional experiments

We replicated the experiments with different models and datasets: the Progressive GAN generator trained on CelebA-HQ and the Improved WGAN unconditional generator with DCGAN architecture trained on CIFAR-10. In both cases we obtain equivalent results (see for example Figure 11).

## Additional applications

Besides the proposed unsupervised segmentation, our method can be applied for manipulation of general *real* images (e.g. interpolation between images, class switching, etc.). See Figs. 11, 12 and third row of Fig. 14.

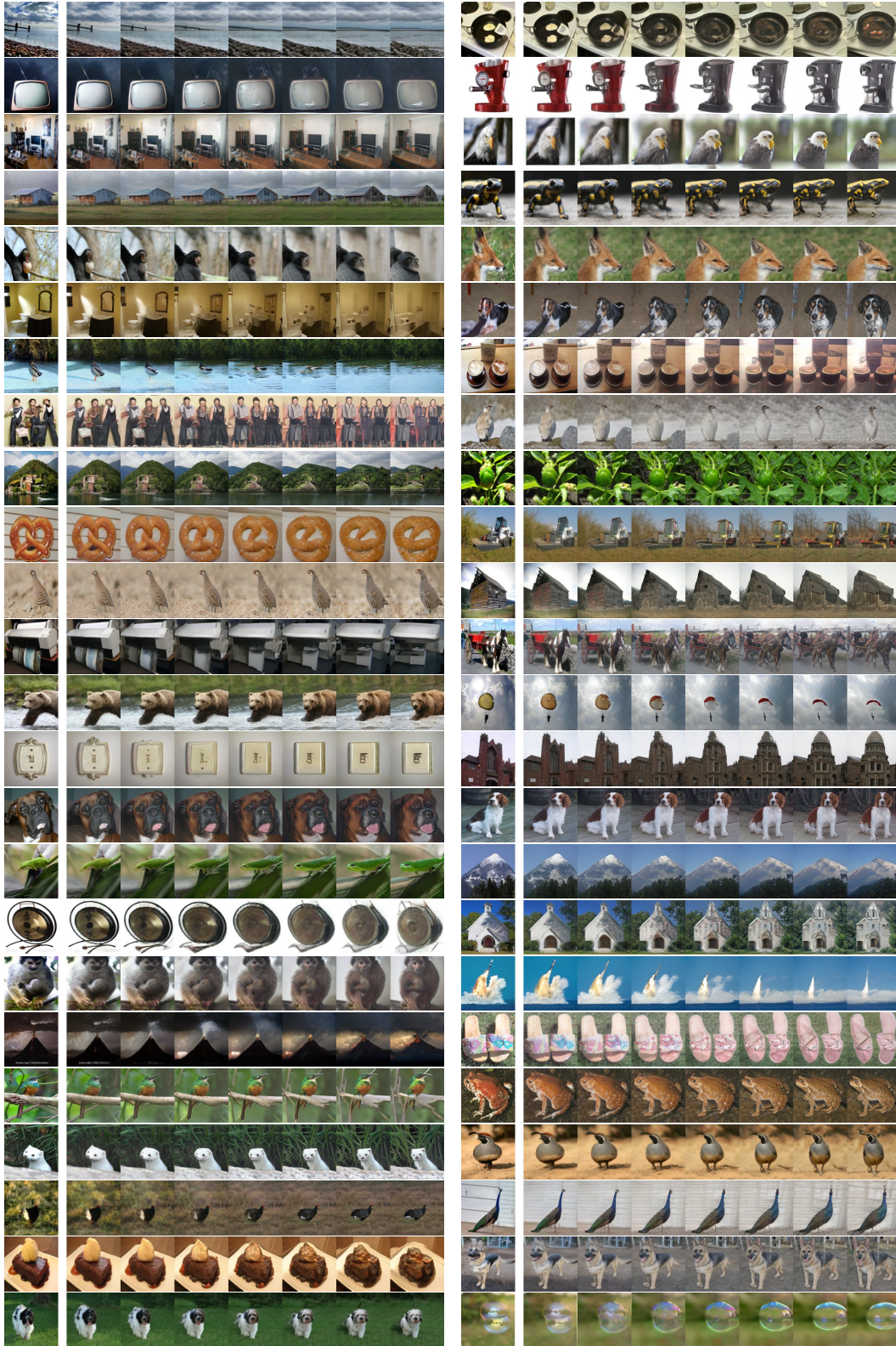


Figure 7: Left: Real image. Right: Linear interpolation between its closest reconstruction in the first step of the optimization ( $G_2(G_1(z^*))$ , right) and the closest reconstruction in the second step ( $G_2(G_1(z^*) + \delta^*)$ , left). Note that except from the right-most column, the rest of intermediate images can not be generated from the latent space.

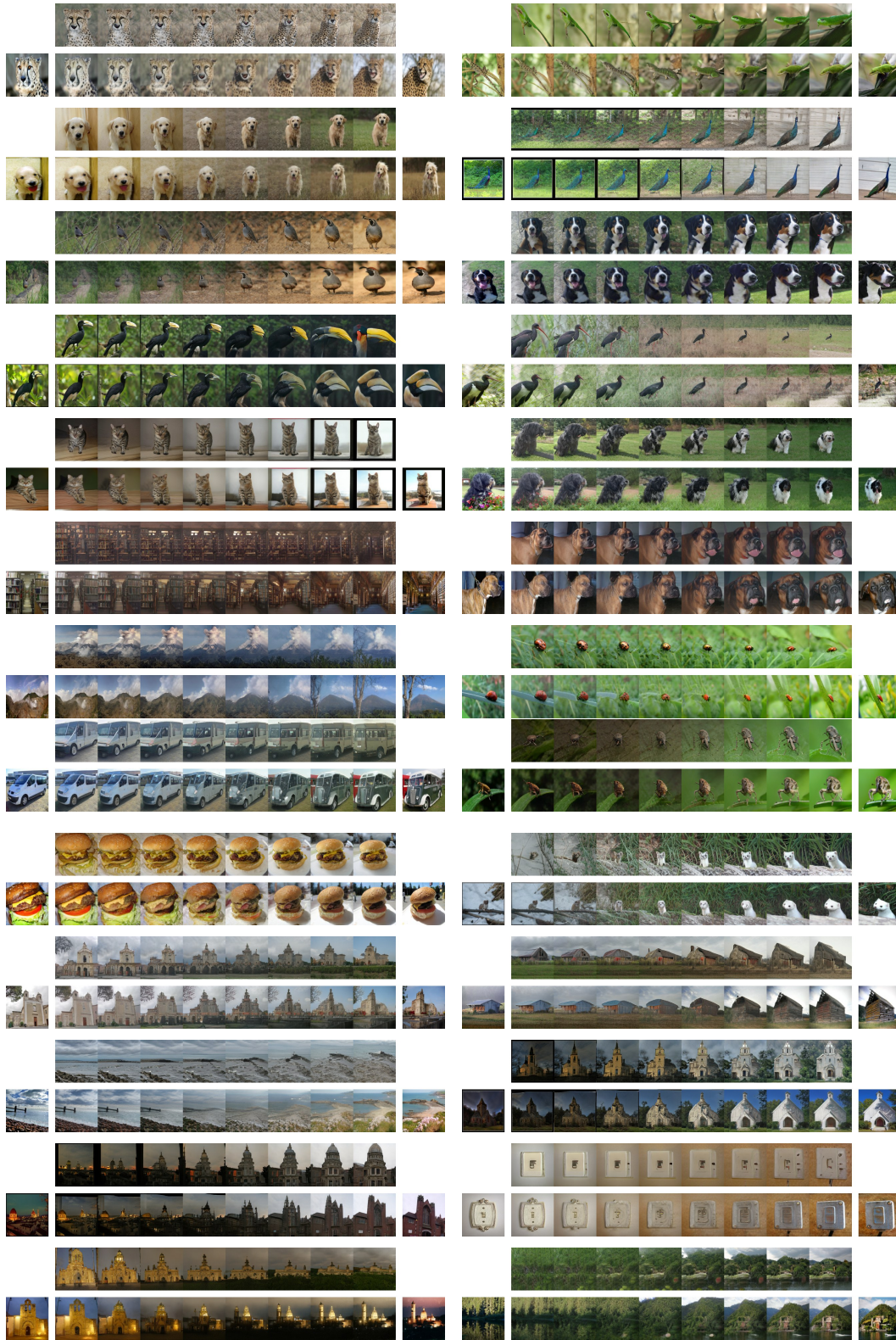


Figure 8: Linear interpolation between the reconstruction of two real images for the same class. First row: reconstruction in the latent space. Second row: reconstruction in the dense layer with the proposed two-step optimization.



Figure 9: Linear interpolation in the space of the dense layer, between the reconstruction of a real image (left) and a random generated image in the same class (right). Note that except from the right-most column, the rest of intermediate images can not be generated from the latent space.

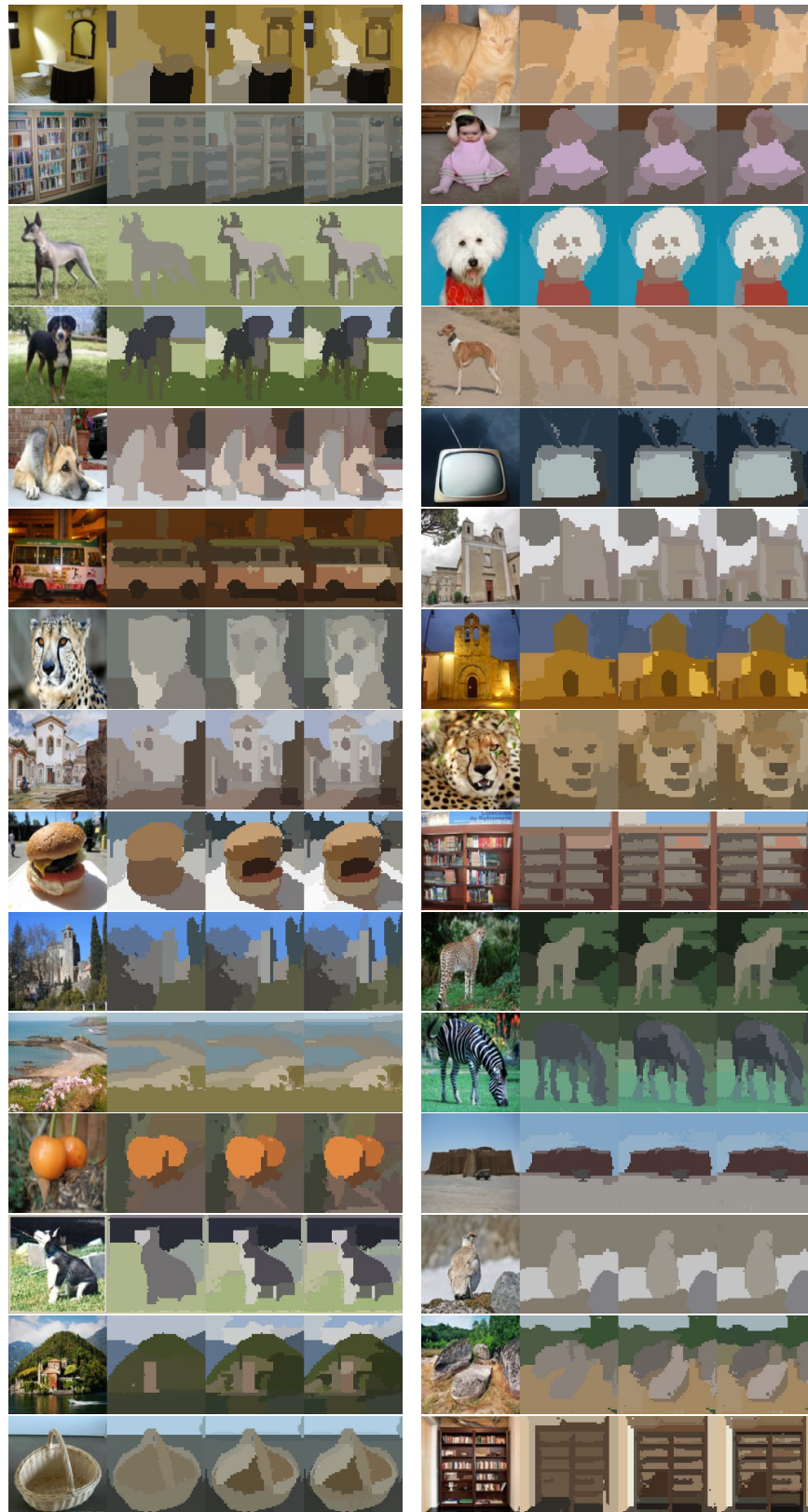


Figure 10: Examples of unsupervised segmentation (64x64) for real images, after inverting the generator to the first layer (different numbers of clusters: 8, 20, 40). Only for visualization purposes, each cluster is associated to the average color of all its pixel members.



Figure 11: Linear interpolation between the reconstruction of two real images (First row: the latent space. Second row: the dense layer). Top: Progressive GAN on CelebA-HQ. Bottom: Improved WGAN on CIFAR-10.



Figure 12: Illustrative practical application of our method (BigGAN). First row: original sequence of frames. Second row: reconstruction in the first dense layer. Third and Fourth row: reconstruction after changing the input class.



Figure 13: Top: Real images. Middle: Reconstruction in the dense layer ( $h^*$ ). Bottom: proj of  $h^*$  onto  $G_1(\mathcal{Z})$ .

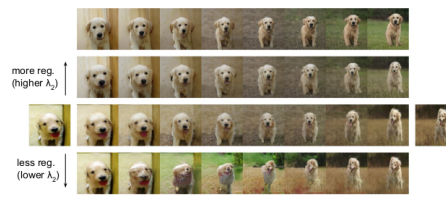


Figure 14: Effects of regularization in the interpolation quality (top row: interpolation in the latent space).